Texture Analysis of the Retinal Nerve Fiber Layer in Fundus Images via Markov Random Fields

R. Kolář[1] and P. Vácha[2]

[1] Department of Biomedical Engineering, Brno University of Technology, Brno, Czech Republic
[2] Institute of Information Theory and Automation of the ASCR, Prague, Czech Republic

Abstract— **This paper describes method for analysis of the texture created by retinal nerve fibers (RNF) via Markov Random Fields. The Causal Autoregressive Random (CAR) model is used to create a feature vector describing the changes in texture due to losses in RNF layer. It is shown that features based on CAR model can be used for discrimination between healthy and glaucomatous tissue using simple linear classifier. The classification error is slightly below 4% for the tested dataset.**

Keywords— **glaucoma, texture analysis, fundus image.**

I. Introduction

Glaucoma is the second most frequent cause of permanent blindness in industrial developed countries. During glaucoma progression, the degeneration of retinal ganglia cells, axons and gliocells are damaged. If not diagnosed in early stage, the damage of the optical nerve and other structures becomes permanent, which in the final stage may leads to blindness. One of the glaucoma symptoms is the graduall loss of the retinal nerve fibers (RNF), which has been proved of high diagnostic value. The RNF atrophy is indicated as a texture changes in colour or greyscale retinal photographs. Therefore, there has been a high effort to use these retinal images to evaluate a RNF since 1980 [1]. But until now, there is no routinely used method for RNF quantification (based only on colour photography), although an increasing effort in this field is noticeable [2, 3, 4].

Although, expansion of the new technologies in diagnosis process is increasing, the diagnosis based only on color fundus photographs is important, because digital color fundus camera has became a standard tool for fundus examination [5, 6, 7] and the resolution of acquired image is sufficient for detection of fine structures created by retinal nerve fibers.

This paper presents new features for RNF analysis, using Markov random fields, applied to the texture created by RNF layer. Section 2 describes the images and their properties with respect to RNF analysis. Section 3 shortly introduces the MRF and its application to texture description. Also feature selection is shortly discussed. The results, based on two different classifiers are presented and discussed in Section 4. Section 5 concludes this paper.

II. Data

The database contain 16 color images of glaucomatous eyes with focal RNF loss and 14 color images of healthy eyes in JPEG format with very low compression. Green and blue channels were extracted from these images taken by fundus camera (Canon CF-60UDi with digital camera Canon D20). The mean value from green and blue channels was computed, because the red component doesn't carry any information from RNF layer. This is contained only on the corresponding green-blue wavelengths of reflected eye.

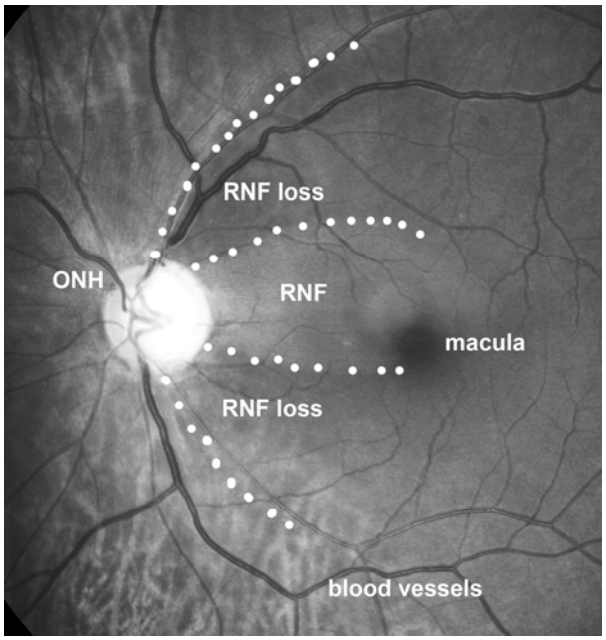

Fig. 1 One image from our database showing macula, optic nerve head (ONH), blood vessels and areas with/without retinal nerve fibers.

The size of the images is 3504 x 2336 pixels with a large field of view (60°). One image from that database with RNF loss is shown in Fig. 1, depicting the main struc-

O. Dössel and W.C. Schlegel (Eds.): WC 2009, IFMBE Proceedings 25/XI, pp. 247–250, 2009.
www.springerlink.com

tures and also two areas with RNF losses. Optical nerve head (ONH) is a place where blood vessels and RNF enters or leaves the inner eye. The macula is the place with the highest concentration of retinal ganglia cells. The RNF runs mainly from the ONH to macula with the highest concentration in radial direction.

The RNF losses appear as a darker area, which is caused by decreasing number of the nerve fiber bundles and lowering the reflection of incident light. As the reflection depends on the optical properties of the examined eye, the brightness is not a reliable feature for RNF description. The RNFL are represented as a striation pattern, which creates texture - the neural fibers are locally oriented in parallel, which causes their lightly stripy appearance.

The testing of the new features was done on the three databases of samples. The small square samples (41x41 pixels) were selected from the retinal images for texture analysis:

- image samples *with* tissues containing the RNF (304 samples, class **A**) from patients with glaucoma.
- image samples from area *without* RNF (176 samples, class **B**) from patients with glaucoma.
- image samples from control group - samples selected from healthy eyes of patients without glaucoma (227 samples, class **C**).

The size of these samples was selected in order to span a sufficiently large region with RNF striation. The maximum size was limited by the blood vessels and other anatomical and pathological structure in the retinal image. Their positions were selected in close surrounding around ONH, not exceeding double radius of the ONH from ONH border. Value of pixels in all samples were normalized to the range of 1 to 64 before further processing to eliminate different illumination conditions caused by the different optical eye properties.

III. Method

A. Markov Random Fields

Markov Random Fields (MRF) were successfully used for illumination a brightness insensitive texture recognition [8, 9]. We start the analysis of texture T with a computation of gradient image $[\partial_{r1} T(r), \partial_{r2} T(r)] = [T(r_1+1, r_2) - T(r_1-1, r_2), T(r_1, r_2+1) - T(r_1, r_2-1)]$ for each pixel $r = (r_1, r_2)$, where the first component r_1 of the multiindex r is the row and r_2 is the column index, respectively. Subsequently, the Gaussian pyramid with two levels is computed and each pyramid level is modelled by a Markov Random Field type of model - the Causal Autoregressive Random (CAR) model [10,11]. The each partial derivation is modelled separately using a 2-dimensional CAR model.

The CAR representation assumes that pixel value Y_r can be modelled as a linear combination of its neighbours:

$$Y_r = \sum_{s \in I_r} a_s Y_{r-s} + \varepsilon_r \ ,$$

where r, s are multiindeces and some selected contextual unilateral neighbour index shift set is denoted I_r, η is the size of I_r. We used the 3rd order hierarchical neighbourhood (η=6) depicted in Fig 2. The model parameters a_s are unknown and they represent appearance of the texture. The white noise ε_r has normal density with zero mean, unknown variance σ^2 independent of previous data and same for every position r.

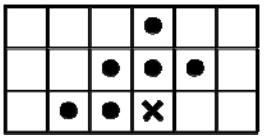

Fig. 2 Diagram of the 3rd order unilateral hierarchical neighbourhood, the actual pixel is denoted as X.

Using this type of neighbourhood, the estimate of CAR parameters σ^2, a_s, $s = 1 \ldots \eta$, can be expressed analytically and computed using fast, numerically robust and recursive statistics [12]. The model analyses texture in a chosen direction of movement, one pixel after another pixel, and the parameter estimate is updated at each pixel position r according to its value Y_r and values of its neighbors Y_{r-s}. We used more movement directions, to capture supplementary texture properties, all used directions were row-wise top-down, row-wise bottom-up and column-wise left-right.

Finally, the estimated model parameters σ^2, a_s, $s = 1 \ldots \eta$, for both partial derivations of image gradient, all three directions and two levels of Gaussian pyramid are concatenated into a common feature vector *f*.

B. Feature Selection and Classification

The feature selection has been performed in the sense of Maximum Relevance and Minimum Redundancy (MRMR) approach [13]. This scheme is based on two concepts: a *good* feature should have maximum relevance to target class and minimum redundancy to already selected features. These two properties can be described by mutual information.

The features selection works in an iterative manner. First, the feature with the highest mutual information is selected. The rest features are selected incrementally, e.g. previously selected features stay in a new subset and the new feature is selected in such way, that it maximizes MRMR criterion [14]. This approach was applied to all combination of

classes (A-C, B-C, A-B), providing different features for each pair. The best features for each pair of classes were then tested using classifier to evaluate relevance of each feature from classification point of view. Two classifiers were used: the nonlinear Support Vector Machine (SVM) classifier and linear Ho-Kashyap classifier.

The SVM [15] is generalized classifier that maximizes the geometrical margin between the considered classes. The υ-SVM variant was used with the radial basis non-linear transformation (γ=0.5). The classifier was tested in the range of the penalization parameter υ and it was observed that for υ changing from 0.2 to 0.7 the classification error was almost constant. Value υ=0.5 was used for the next tests.

Ho-Kashyap classifier [16] combines perceptron and least mean squared (LMS) classification. This classifier ensures that either separating hyperplane is computed (if available) or LMS optimal solution is found from training data.

The random K-fold cross-validation method was utilized to test the performance of these two classifiers. This procedure takes randomly selected K-folds for training (200 samples) and different K-folds for testing (100 samples). The training and testing samples were run 100 times for different sets to evaluate the classification error.

IV. Results and Discussion

The features from feature vector *f* were sorted according to the criteria defined by MRMR approach. The five most relevant features for each pair of classes (B-C, A-C and A-B) were selected (see Table 1) and further analyzed in the sense of classification accuracy. The parameter f_{19} and f_7 appears in all cases at the top of the ordered sequences. These parameters belongs to relative positions [-1,0] and [-2,0] in model neighbourhood (Fig. 2).

Table 1 Seven best features from CAR model ordered by MRMR approach

	Class B–C	Class A–C	Class A–B
Indexes *i* for parameters in feature vector *f*	3, **19**, **7**, 37, 31, 22, 25	**19**, **7**, 5, 61, 37, 31, 10	45, 9, 11, 24, **19, 7**, 58

The classifiers were used successively for these best features, starting with the most relevant feature, then adding the second most relevant feature etc. The results of classification are presented in Table 2 for different combinations of classes and two tested classifiers.

First results can be formulated by comparing the result of SVM and Ho-Kashyap classifier. The linear classifier performs better on our datasets in all cases.

The second result deals with classification between classes. The classification error decreases with the number of features used for classification as expected. The best results for each pair of classes are boldfaced marked. The number of features ranges from 5 to 7 for different combination of classes. Using more features increases classification error (for Ho-Kashyap classifier) or causes error fluctuation with changing standard deviation.

The 2D feature space for f_{19} and f_7 is presented in Fig. 3 as an example of appropriate features for all combination of classes. Class B and C creates a well separated clusters, which means that we can differentiate between the regions with RNF layer losses and healthy tissue (which is given by healthy population). The cluster for class A is also well separated with respect to class C. Clusters for classes A and B overlaps each other for these features.

Table 2 Classification errors [%] for two classifiers and five most relevant features (different for each pair of classes). Boldfaced numbers indicates the best classification results.

	Classifier	Class B–C	Class A–C	Class A–B
1	Ho-Kashyap	9.21±2.71	17.75±3.57	31.65±3.63
	SVM	28.40±28.71	40.89±18.96	49.78±14.76
1, 2	Ho-Kashyap	6.69±2.32	14.09±3.31	28.49±3.53
	SVM	8.67±2.54	31.59±21.49	44.65±13.36
1, 2, 3	Ho-Kashyap	4.80±2.15	13.45±3.10	26.70±3.84
	SVM	7.28±2.90	20.73±13.10	39.26±12.99
1, 2, 3, 4	Ho-Kashyap	4.78±1.89	13.20±3.23	24.50±3.77
	SVM	7.73±3.09	19.91±13.51	39.47±12.77
1, 2, 3, 4, 5	**Ho-Kashyap**	4.96±1.82	13.21±3.15	**23.40±3.72**
	SVM	7.80±2.81	19.54±15.16	39.58±12.21
1, 2, 3, 4, 5,6	**Ho-Kashyap**	**3.97±1.91**	13.59±3.40	23.75±3.42
	SVM	6.31±3.26	17.25±9.24	35.47±12.31
1, 2, 3, 4, 5,6,7	**Ho-Kashyap**	4.09±2.03	**11.58±2.83**	23.63±3.72
	SVM	6.4±2.82	13.40±4.34	34.59±12.93

V. Conclusion

Results of presented approach indicate that CAR model can be used for detection of the focal losses in RNF layer in connection with the machine learning approach. The classification error for our dataset reached 3.97% for discrimination between regions from healthy tissue and regions from tissue without RNF layer.

The proposed features from CAR model may be used as a part of feature vector in Glaucoma Risk Index, as described in [17]. These features can be also used in the screening program together with other features, based on different texture analysis methods [18, 19] and uses large database of healthy eyes as a control (reference) group.

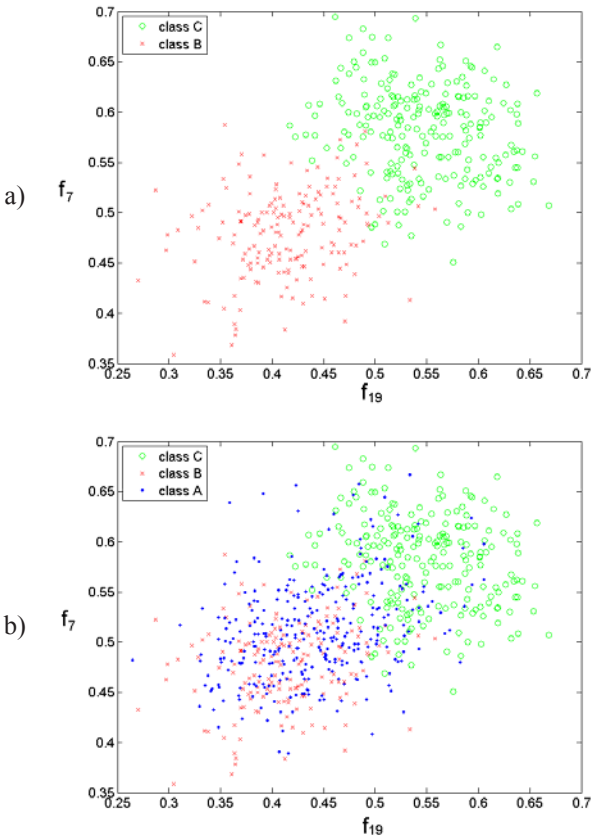

Fig. 3 Feature space for f_{19} and f_7

Acknowledgment

This work has been supported by the DAR - research center no. 1M0572 coordinated by the Institute of Information Theory and Automation of the Czech Academy Science, partly also by the institutional research frame no. MSM 0021630513 (both grants sponsored by the Ministry of Education of the Czech Republic) and partly by grant no. 2C06019. The authors highly acknowledge providing the test set of images by Eye Clinic of MUDr. Kubena in Zlin (Czech Republic).

References

1. Peli E, Hedges TR., Schwartz B (1989) Computer measurement of the retina nerve fiber layer striations. Applied Optics, 28:1128 - 1134
2. Lee S et al. (2004) Automated quantification of retinal nerve fiber layer atrophy in fundus photograph. In 26th Annual International Conference of the IEEE IEMBS, San Francisco, USA, 2004, p. 1241 – 1243
3. Oliva AM, Richards D, Saxon W (2007) Search for color-dependent nerve-fiber-layer thinning in glaucoma: A pilot study using digital imaging techniques. ARVO meeting, Fort Lauderdale, USA, 2007, e-Abstract 3309, at http://www.arvo.org
4. Tornow RP, Laemmer R, Mardin ChY (2008) Quantitative imaging using a fundus camera. ARVO meeting, Fort Lauderdale, USA, 2007, e-Abstract 1206, at http://www.arvo.org.
5. Tuulonen A. et al. (2000) Digital imaging and microtexture analysis of the nerve fibre layer, Journal of Glaucoma, 9:5–9
6. Kolář R, Jan J, Detection of Glaucomatous Eye via Color Fundus Images Using Fractal Dimensions, Radioengineering, vol. 17(3), pp. 109-114, Nov. 2008.
7. Hayashi et al. (2007), "Detection of Retinal Nerve Fiber Layer Defects in Retinal Fundus Images using Gabor Filtering," in Proc. of SPIE, vol. 6514, pp. 65142Z.
8. Vacha P, Haindl M (2008) Illumination Invariants Based on Markov Random Fields, in Proc. of the 19th International Conference on Pattern Recognition (ICPR'08), 2008
9. Vacha P., Haindl M (2007) Image Retrieval Measures Based on Illumination Invariant Textural MRF Features, in Proc. of the 6th ACM International Conference on Image and Video Retrieval 2007 (CIVR'07), pp. 448-455, 2007
10. Haindl M. (1991) Texture synthesis, CWI Quarterly, no. 4, vol. 4, pp. 305-331
11. Haindl M. (1999) Texture segmentation using recursive Markov random field parameter estimation, in *Proc. of the 11th Scandinavian Conference on Image Analysis*, pp. 771-776
12. Haindl M., Šimberová S. (1992) Theory & Applications of Image Analysis, chapter A Multispectral Image Line Reconstruction Method, pages 306-315, World Scientific Publishing Co., Singapore
13. Peng H, Long F, Ding Ch (2005) Feature selection based on mutual information: Criteria of max-dependency, max-relevance and min-redundancy, IEEE Transaction on Pattern Analysis and Machine Intelligence 27(8):1226-1238
14. Ding Ch, Peng H (2005) Minimum redundancy feature selection from microarray gene expression data, Journal of Bioinformatics and Computational Biology 3(2):185-205
15. Chang Ch, Lin Ch J (2008) *LIBSVM - A Library for Support Vector Machines* at http://www.csie.ntu.edu.tw/~cjlin/libsvm
16. Duda RO, Hart PE, Stork D (2000) Pattern Classification, New York: John Wiley & Sons.
17. Bock R., Meier J., Michelson G., Nyul L.G., Hornegger J. (2007) Classifying glaucoma with image-based features from fundus photographs. *Lecture Notes in Computer Science*, Springer, vol. 4713, pp. 355 – 365
18. Kolář, R., Urbánek, D., Jan, J. (2008) Texture based discrimination of normal and glaucomatous retina. *In Analysis of Biomedical Signals and Images*, Biosignal 2008, Brno, Czech Republic, CD-ROM proceedings, 5 pages
19. Gazárek J., Jan, J., Kolář, R. (2008) Detection of neural fibre layer in retina images via textural analysis. *In Analysis of Biomedical Signals and Images*, Biosignal 2008, Brno, Czech Republic, CD-ROM proceedings, 7 pages

Author: Radim Kolář
Institute: Department of Biomedical Engineering, FEEC, Bno University of Technology
Street: Kolejní 4
City: Brno
Country: Czech Republic
Email: kolarr@feec.vutbr.cz